ANNALS of Faculty Engineering Hunedoara – International Journal of Engineering
Tome XX [2022] | Fascicule 3 [August]

[1.] Olimpiu STOICUTA, [2.]Teodor PANA

# COMPARATIVE STUDY OF THREE ADAPTIVE OBSERVERS FOR SENSORLESS VECTOR CONTROL SYSTEMS

[1.] Faculty of Mechanical and Electrical Engineering, University of Petrosani, Petrosani, ROMANIA
[2.]Faculty of Electrical Engineering, Technical University of Cluj-Napoca, Cluj-Napoca, ROMANIA

**Abstract:** The paper presents a comparison between three different techniques for simultaneously estimating the speed, position and rotor flux modulus of an induction motor, which is used in a sensorless vector control system. The comparison highlights the dynamic performances, as well as the stability of the obervers in the area of low speeds. Dynamic performances testing is done by simulation using the Matlab-Simulink program.
**Keywords:** induction motors, observers, stability analysis, numerical simulation, sensorless vector control system

## 1. MATHEMATICAL MODEL OF THE INDUCTION MOTOR

The equations defining the mathematical model of the induction motor are [1]

$$\frac{d}{dt}\begin{bmatrix}\underline{i}_s\\ \underline{\psi}_r\end{bmatrix}=\begin{bmatrix}a_{11} & a_{13}-j\cdot a_{14}\cdot z_p\cdot\omega_r\\ a_{31} & a_{33}+j\cdot z_p\cdot\omega_r\end{bmatrix}\cdot\begin{bmatrix}\underline{i}_s\\ \underline{\psi}_r\end{bmatrix}+\begin{bmatrix}b_{11}\\ 0\end{bmatrix}\cdot\underline{u}_s \tag{1}$$

$$J_m\cdot\frac{d\omega_r}{dt}=T_M-T_F-F\cdot\omega_r-T_L \tag{2}$$

where:

$$\underline{i}_s=i_{ds}+j\cdot i_{qs};\ \underline{\psi}_r=\psi_{dr}+j\cdot\psi_{qr};\ \underline{\psi}_r^*=\psi_{dr}-j\cdot\psi_{qr};\ \underline{u}_s=u_{ds}+j\cdot u_{qs};\ j=\sqrt{-1};\ T_M=K_T\cdot\mathrm{Im}\left(\underline{\psi}_r^*\cdot\underline{i}_s\right);$$

$$a_{11}=-\left(\frac{1}{T_s\cdot\sigma}+\frac{1-\sigma}{T_r\cdot\sigma}\right);\ a_{13}=\frac{L_m}{L_s\cdot L_r\cdot T_r\cdot\sigma};\ a_{14}=\frac{L_m}{L_s\cdot L_r\cdot\sigma};\ a_{31}=\frac{L_m}{T_r};\ a_{33}=-\frac{1}{T_r};\ b_{11}=\frac{1}{L_s\cdot\sigma};T_s=\frac{L_s}{R_s};$$

$$T_r=\frac{L_r}{R_r};\sigma=1-\frac{L_m^2}{L_s\cdot L_r};K_T=\frac{3}{2}\cdot z_p\cdot\frac{L_m}{L_r};\ \omega=z_p\cdot\omega_r.$$

In the above relationships, the following notations are used: $R_s$, $R_r$ – stator and rotor resistances; $L_s$, $L_r$ – stator and rotor self-inductances; $L_m$ – mutual inductance; $T_s$, $T_r$ – stator and rotor time-constants; $\sigma$ – leakage coefficient; $z_p$ – number of pole pairs; $J_m$ – moment of inertia of the rotor; $F$ – friction coefficient; $K_T$ – torque constant; $T_M$ – instantaneous electromagnetic torque of the motor; $T_F$ – static friction torque; $F$ – the coefficient of viscous friction; $T_L$ – load torque; $\omega_r$ – mechanical angular speed of the rotor; $\omega$ – electric angular speed of the rotor; $\underline{i}_s$ – space vector of the stator current; $\underline{\psi}_r$ – space vector of the rotor flux; $\underline{u}_s$ – space vector of the stator voltage; *Im (x)* - the imaginary part of *x*.

## 2. EXTENDED LUENBERGER OBERVER (ELO)

The equations that define the rotor flux Luenberger observer are [2]

$$\frac{d\hat{x}}{dt}=A\cdot\hat{x}+B\cdot u+L\cdot C\cdot\left(x-\hat{x}\right) \tag{3}$$

where: $A=\begin{bmatrix}a_{11} & a_{13}-j\cdot a_{14}\cdot z_p\cdot\hat{\omega}_r\\ a_{31} & a_{33}+j\cdot z_p\cdot\hat{\omega}_r\end{bmatrix}$; $C=\begin{bmatrix}1 & 0\end{bmatrix}$; $\hat{x}=\begin{bmatrix}\hat{\underline{i}}_s & \hat{\underline{\psi}}_r\end{bmatrix}^T$; $u=\underline{u}_s$.

The coefficients of the Luenberger amplification matrix are:

$$L=\begin{bmatrix}l_{11}+j\cdot l_{12}\\ l_{21}+j\cdot l_{22}\end{bmatrix} \tag{4}$$

The elements of Luenberger matrix are [2]:

$$\begin{cases}la_{11}=\left(1-k\right)\cdot\left(a_{11}+a_{33}\right)\\ la_{12}=z_p\cdot\hat{\omega}_r\cdot\left(1-k\right)\\ la_{22}=-\gamma\cdot la_{12}\\ la_{21}=\left(a_{31}+\gamma\cdot a_{11}\right)\cdot\left(1-k^2\right)-\gamma\cdot la_{11}\end{cases} \tag{5}$$

where $\gamma = 1/a_{14}$, and $k$ is the proportionality factor between the eigenvalues of the estimator and the eigenvalues of the induction machine ($k > 0$).

From relations (3) and (5) is observed that the matrices *A* and *L* adaptation according to the rotor speed, which is estimated with the speed observer.

The equations that define the speed observer are [2]

$$\hat{\omega}_r(t) = K_{Ra} \cdot f(t) + K_{Ia} \cdot \int_0^t f(\tau)\, d\tau \tag{6}$$

where: $f(t) = e_a(t) \cdot \hat{\psi}_{qr}(t) - e_b(t) \cdot \hat{\psi}_{dr}(t)$; $e_a(t) = i_{ds}(t) - \hat{i}_{ds}(t)$; $e_b(t) = i_{qs}(t) - \hat{i}_{qs}(t)$.

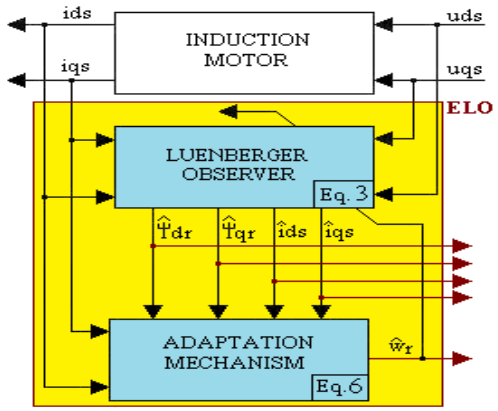


Figure 1. The Extended Luenberger Observer (ELO)

In the above relation, $K_{Ra}$ and $K_{Ia}$ constants are chosen to obtain the desired dynamic regime. The block diagram of the extended Luenberger observer (ELO) is presented in Figure 1.

## 3. SOC OBERVER

The following relation defines the rotor flux observer [3], [4]:

$$\frac{dx}{dt} = A \cdot x + B \cdot u + G \cdot C \cdot \left( \frac{dx}{dt} - \frac{dx}{dt} \right) \tag{7}$$

where: $A = \begin{bmatrix} a_{11} & a_{13} - j \cdot a_{14} \cdot z_p \cdot \hat{\omega}_r \\ a_{31} & a_{33} + j \cdot z_p \cdot \hat{\omega}_r \end{bmatrix}$; $G = \begin{bmatrix} g_{11} + j \cdot g_{12} \\ g_{21} + j \cdot g_{22} \end{bmatrix}$;

$C = \begin{bmatrix} 1 & 0 \end{bmatrix}$; $\hat{x} = \begin{bmatrix} \underline{\hat{i}}_s & \underline{\hat{\psi}}_r \end{bmatrix}^T$; $u = \underline{u}_s$.

The elements of G matrix are:

≡ Variant 1[3]

$$\begin{cases} g_{11} = \dfrac{1-k^2}{k^2}; \\ g_{12} = 0 \end{cases} \quad \begin{cases} g_{21} = \dfrac{k-1}{a_{14} \cdot k^2} - g_{22} \cdot \dfrac{a_{33}}{z_p \cdot \hat{\omega}_r} \\ g_{22} = \dfrac{k-1}{k} \cdot \dfrac{a_{11}}{a_{14}} \cdot \dfrac{z_p \cdot \hat{\omega}_r}{z_p^2 \cdot \hat{\omega}_r^2 + a_{33}^2} \end{cases} \tag{8}$$

≡ Variant 2 [4]

$$\begin{cases} g_{11} = -\left( 1 + \dfrac{1}{k^2} \cdot \dfrac{z_p^2 \cdot \hat{\omega}_r^2 - a_{33}^2}{z_p^2 \cdot \hat{\omega}_r^2 + a_{33}^2} \right); \\ g_{12} = \dfrac{2 \cdot a_{33}}{k^2} \cdot \dfrac{z_p \cdot \hat{\omega}_r}{z_p^2 \cdot \hat{\omega}_r^2 + a_{33}^2} \end{cases} \quad \begin{cases} g_{21} = \dfrac{1}{a_{14}} \cdot \left( \dfrac{1-k}{k} - g_{11} + \dfrac{a_{11} \cdot k \cdot (1-k)}{2 \cdot z_p \cdot \hat{\omega}_r} \cdot g_{12} \right) \\ g_{22} = \dfrac{a_{11} \cdot k \cdot (k+1) - 2 \cdot a_{33}}{2 \cdot a_{33} \cdot a_{14}} \cdot g_{12} \end{cases} \tag{9}$$

The equations that define the speed observer are [3], [4]

$$\hat{\omega}_r(t) = K_{Rb} \cdot g(t) + K_{Ib} \cdot \int_0^t g(\tau)\, d\tau \tag{10}$$

where: $g(t) = e_a(t) \cdot \hat{\psi}_{qr}(t) - e_b(t) \cdot \hat{\psi}_{dr}(t)$; $e_a(t) = i_{ds}(t) - \hat{i}_{ds}(t)$; $e_b(t) = i_{qs}(t) - \hat{i}_{qs}(t)$.

In the above relation, $K_{Rb}$ and $K_{Ib}$ constants are chosen to obtain the desired dynamic regime.

## 4. THE GOPINATH-PENG OBERVER

The estimation of the position and modulus the space vector of the rotor flux is doing with the help of a reduced order Gopinath observer [5]. The equation, which define the Gopinath observer, is:

$$\frac{d\underline{\hat{\psi}}_r}{dt} = S_a + \underline{G} \cdot \left( \frac{d\underline{i}_s}{dt} - C_a \right) \tag{11}$$

where: $S_a = A_{21} \cdot \underline{i}_s + \tilde{A}_{22} \cdot \underline{\hat{\psi}}_r$; $C_a = A_{11} \cdot \underline{i}_s + \tilde{A}_{12} \cdot \underline{\hat{\psi}}_r + b_{11} \cdot \underline{u}_s$; $A_{11} = a_{11}$; $\tilde{A}_{12} = a_{13} - j \cdot a_{14} \cdot z_p \cdot \hat{\omega}_r$; $A_{21} = a_{31}$; $\tilde{A}_{22} = a_{33} + j \cdot z_p \cdot \hat{\omega}_r$.

The Gopinath observer gain is [5]

$$\underline{G} = G_d + j \cdot G_q \tag{12}$$

where:

$$\begin{cases} G_d = -\dfrac{1}{a_{14}} \cdot \left( 1 + \dfrac{k \cdot a_{33}}{\sqrt{a_{33}^2 + \left( z_p \cdot \hat{\omega}_r \right)^2}} \right) \\ G_q = \dfrac{1}{a_{14}} \cdot \dfrac{k \cdot z_p \cdot \hat{\omega}_r}{\sqrt{a_{33}^2 + \left( z_p \cdot \hat{\omega}_r \right)^2}} \end{cases} \tag{13}$$

The block diagram of the Gopinath observer is in Figure 2. The block diagram of the speed and rotor flux observer is in Figure 3.

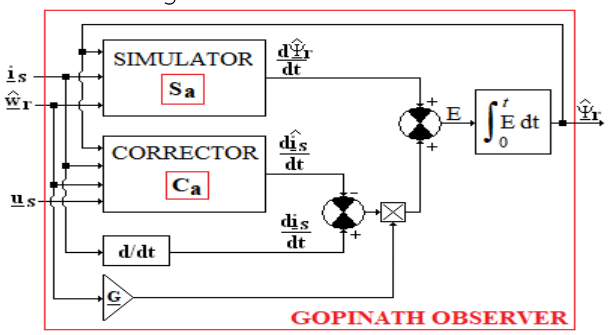


Figure 2. The Gopinath observer

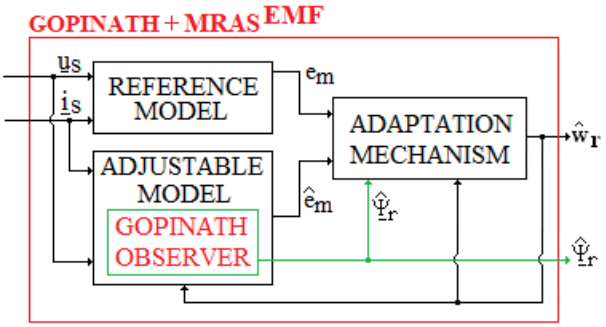


Figure 3. The Gopinat + MRAS$^{EMF}$ speed observer

The speed of the induction motor is estimated using a back-EMF MRAS speed observer (Peng observer [6]), defined by the following equations [7]:

≡ The reference model

$$\underline{e}_m = \underline{u}_s - R_s \cdot \underline{i}_s - \sigma \cdot L_s \cdot \frac{d\underline{i}_s}{dt} \tag{14}$$

where $\underline{e}_m = e_{dm} + j \cdot e_{qm}$ is the real rotor back electromotive force space vector.

≡ The adjustable model [7]

$$\hat{\underline{e}}_m = \frac{L_m}{L_r} \cdot \frac{d\hat{\underline{\psi}}_r}{dt} \tag{15}$$

where $\hat{\underline{e}}_m = \hat{e}_{dm} + j \cdot \hat{e}_{qm}$ is the estimated rotor back electromotive force space vector.

Using the relation (11), the adjustable model becomes [7]

$$\hat{\underline{e}}_m = \frac{L_m}{L_r} \cdot \left( S_a + \underline{G} \cdot \left( \frac{d\underline{i}_s}{dt} - C_a \right) \right) \tag{16}$$

≡ The adaptation mechanism [7]

$$\hat{\omega}_r = K_{Rc} \cdot \varepsilon + K_{Ic} \cdot \int_0^t \varepsilon \, dt \tag{17}$$

where: $\varepsilon = -\left( a_{33} \cdot \varepsilon_a + z_p \cdot \hat{\omega}_r \cdot \varepsilon_b \right)$; $\varepsilon_a = \hat{\psi}_{dr} \cdot e_2 - \hat{\psi}_{qr} \cdot e_1$; $\varepsilon_b = \hat{\psi}_{dr} \cdot e_1 + \hat{\psi}_{qr} \cdot e_2$; $e_1 = e_{dm} - \hat{e}_{dm}$; $e_2 = e_{qm} - \hat{e}_{qm}$.

In the (17) relation, $K_{Rc}$ and $K_{Ic}$ constants are chosen to obtain the desired dynamic regime.

## 5. STABILITY ANALYSIS

In the following we analyze the stability of the speed observers presented above (these observers are defined by relations (6), (10) and (17)).

In this sense, all the equations presented above are written in an arbitrary frame of reference that rotates with the electrical angular synchronous speed ($\omega_e$)

$$\omega_e = \omega + \omega_{sl} \tag{18}$$

where: $\omega_e = 2 \cdot \pi \cdot f_e$; $f_e$ - is frequency of three-phase stator voltages applied to the induction motor; $\omega_{sl}$ – is electrical angular slip speed.

Following the linearization of the relationships previously presented around static operating points, we get the following transfer functions:

≡ the transfer function afferent to the Luenberger observer [1]

$$G_1(s) = \frac{\Delta f}{\Delta u} = K_a \cdot \frac{\rho_3 \cdot s^3 + \rho_2 \cdot s^2 + \rho_1 \cdot s + \rho_0}{s^4 + \beta_3 \cdot s^3 + \beta_2 \cdot s^2 + \beta_1 \cdot s + \beta_0} \tag{19}$$

where:

$$K_a = z_p \cdot \underline{\psi}_{r0}^2;\ \underline{\psi}_{r0}^2 = \psi_{dr0}^2 + \psi_{qr0}^2;\ \omega_0 = z_p \cdot \omega_{r0};\ a = z_p \cdot (1-k);\ b = -\gamma \cdot z_p \cdot (1-k);\ \Delta u = \Delta\omega_r - \Delta\hat{\omega}_r;$$

$$\Delta f = \psi_{qr0} \cdot \Delta e_a - \psi_{dr0} \cdot \Delta e_b;\ \omega_{e0} = \omega_0 + \omega_{sl0};\ \rho_3 = a_{14};\ \rho_2 = -2 \cdot a_{14} \cdot a_{33} + a_{14} \cdot la_{11} - a_{13} - a_{11} \cdot a_{14};$$

$$\rho_1 = \left(b \cdot a_{14}^2 \cdot z_p + a \cdot a_{14} \cdot z_p\right) \cdot \omega_{r0}^2 + a_{14} \cdot a_{33}^2 + a_{13} \cdot a_{14} \cdot la_{21} + a_{14} \cdot \omega_{e0}^2 - a_{13} \cdot a_{14} \cdot a_{31} - ;$$
$$- 2 \cdot a_{14} \cdot a_{33} \cdot la_{11} + 2 \cdot a_{11} \cdot a_{14} \cdot a_{33} + a_{11} \cdot a_{13} - a_{13} \cdot la_{11} + a_{13} \cdot a_{33}$$

$$\rho_0 = \left(-a_{11} \cdot a_{14} + a_{13} + a_{14} \cdot la_{11}\right) \cdot \omega_{e0}^2 + \left(a_{11} \cdot a_{14} \cdot z_p + a_{14}^2 \cdot a_{31} \cdot z_p + b \cdot a_{13} \cdot a_{14} + a \cdot a_{13} - \right.$$
$$- a_{14} \cdot a_{33} \cdot z_p - a_{13} \cdot z_p - a_{14}^2 \cdot la_{21} \cdot z_p - a_{14} \cdot la_{11} \cdot z_p \Big) \cdot \omega_{r0} \cdot \omega_{e0} + \left(-b \cdot a_{14}^2 \cdot a_{33} \cdot z_p - b \cdot a_{13} \cdot a_{14} \cdot z_p - \right. ;$$
$$- a \cdot a_{14} \cdot a_{33} \cdot z_p - a \cdot a_{13} \cdot z_p \Big) \cdot \omega_{r0}^2 - a_{13} \cdot a_{14} \cdot la_{21} \cdot a_{33} + a_{14} \cdot a_{33}^2 \cdot la_{11} + a_{13}^2 \cdot a_{31} + a_{13} \cdot a_{14} \cdot a_{31} \cdot a_{33} -$$
$$- a_{11} \cdot a_{14} \cdot a_{33}^2 - a_{13}^2 \cdot la_{21} - a_{11} \cdot a_{13} \cdot a_{33} + a_{13} \cdot a_{33} \cdot la_{11}$$

$$la_{11} = (1-k) \cdot (a_{11} + a_{33});\ la_{12} = z_p \cdot \omega_{r0} \cdot (1-k);\ la_{22} = -\gamma \cdot la_{12};\ la_{21} = \left(a_{31} + \gamma \cdot a_{11}\right) \cdot \left(1-k^2\right) - \gamma \cdot la_{11};$$

$$\beta_3 = 2 \cdot \left(la_{11} - a_{11} - a_{33}\right);$$

$$\beta_2 = \left(a^2 + z_p^2 + 2 \cdot b \cdot a_{14} \cdot z_p\right) \cdot \omega_{r0}^2 + 2 \cdot \left(a - z_p\right) \cdot \omega_{e0} \cdot \omega_{r0} + 2 \cdot \omega_{e0}^2 + la_{11}^2 - 2 \cdot a_{11} \cdot la_{11} - 4 \cdot a_{33} \cdot la_{11} + ;$$
$$+ 2 \cdot a_{13} \cdot la_{21} - 2 \cdot a_{13} \cdot a_{31} + \left(a_{11} + a_{33}\right)^2 + 2 \cdot a_{11} \cdot a_{33}$$

$$\beta_1 = \Big[-2 \cdot a^2 \cdot a_{33} + 2 \cdot \left(z_p^2 + b \cdot a_{14} \cdot z_p\right) \cdot la_{11} - 2 \cdot b \cdot a_{14} \cdot a_{33} \cdot z_p - 2 \cdot b \cdot a_{13} \cdot z_p - 2 \cdot b \cdot a_{11} \cdot a_{14} \cdot z_p -$$
$$-2 \cdot a_{14} \cdot a_{31} \cdot z_p^2 + 2 \cdot a_{14} \cdot la_{21} \cdot z_p^2 - 2 \cdot a \cdot a_{14} \cdot la_{21} \cdot z_p - 2 \cdot a_{11} \cdot z_p^2 + 2 \cdot a \cdot b \cdot a_{13} + 2 \cdot a \cdot a_{14} \cdot a_{31} \cdot z_p \Big] \cdot \omega_{r0}^2 +$$
$$+4 \cdot \left(a_{11} \cdot z_p + b \cdot a_{13} - a_{14} \cdot la_{21} \cdot z_p - la_{11} \cdot z_p - a \cdot a_{33} + a_{14} \cdot a_{31} \cdot z_p\right) \cdot \omega_{r0} \cdot \omega_{e0} + 2 \cdot \left(la_{11} - a_{11} - a_{33}\right) \cdot \omega_{e0}^2 + ;$$
$$+2 \cdot a_{13} \cdot a_{31} \cdot a_{33} + 2 \cdot a_{13} \cdot la_{11} \cdot la_{21} - 2 \cdot a_{13} \cdot a_{33} \cdot la_{21} - 2 \cdot a_{11} \cdot a_{13} \cdot la_{21} - 2 \cdot a_{11}^2 \cdot a_{33} + 4 \cdot a_{11} \cdot a_{33} \cdot la_{11} -$$
$$-2 \cdot a_{13} \cdot a_{31} \cdot la_{11} + 2 \cdot a_{33}^2 \cdot la_{11} + 2 \cdot a_{11} \cdot a_{13} \cdot a_{31} - 2 \cdot a_{33} \cdot la_{11}^2 - 2 \cdot a_{11} \cdot a_{33}^2$$

$$\beta_0 = z_p^2 \cdot \left(2 \cdot a \cdot b \cdot a_{14} + a^2 + b^2 \cdot a_{14}^2\right) \cdot \omega_{r0}^4 + 2\Big[a \cdot z_p \cdot \left(z_p - a\right) + a_{14} \cdot z_p \cdot \left(b \cdot z_p - a \cdot b\right)\Big] \cdot \omega_{e0} \cdot \omega_{r0}^3 +$$
$$+\Big\{\left(a^2 - 2 \cdot b \cdot a_{14} \cdot z_p + z_p^2 - 4 \cdot a \cdot z_p\right)\omega_{e0}^2 + 2a_{14} \cdot la_{11} \cdot la_{21} \cdot z_p^2 - 2b \cdot a_{14} \cdot a_{33} \cdot la_{11} \cdot z_p - 2b \cdot a_{13} \cdot la_{11} \cdot z_p -$$
$$-2 \cdot a_{31} \cdot a_{14} \cdot la_{11} \cdot z_p^2 - 2 \cdot a_{11} \cdot la_{11} \cdot z_p^2 - 2 \cdot a_{11} \cdot a_{14} \cdot la_{21} \cdot z_p^2 + 2 \cdot b \cdot a_{11} \cdot a_{13} \cdot z_p + 2 \cdot a_{11} \cdot a_{14} \cdot a_{31} \cdot z_p^2 +$$
$$+la_{11}^2 \cdot z_p^2 + 2 \cdot b \cdot a_{11} \cdot a_{14} \cdot a_{33} \cdot z_p + 2 \cdot a \cdot a_{13} \cdot la_{21} \cdot z_p + a^2 \cdot a_{33}^2 + a_{11}^2 \cdot z_p^2 - 2 \cdot a \cdot b \cdot a_{13} \cdot a_{33} + b^2 \cdot a_{13}^2 -$$
$$-2 \cdot a \cdot a_{14} \cdot a_{31} \cdot a_{33} \cdot z_p - 2 \cdot a \cdot a_{13} \cdot a_{31} \cdot z_p + 2 \cdot a \cdot a_{14} \cdot a_{33} \cdot la_{21} \cdot z_p + a_{14}^2 \cdot la_{21}^2 \cdot z_p^2 - 2 \cdot a_{14}^2 \cdot a_{31} \cdot la_{21} \cdot z_p^2 +$$
$$+a_{14}^2 \cdot a_{31}^2 \cdot z_p^2\Big\} \cdot \omega_{r0}^2 + \Big\{2 \cdot \left(a - z_p\right) \cdot \omega_{e0}^3 + \Big[-2 \cdot b \cdot a_{11} \cdot a_{13} + 2 \cdot a_{14} \cdot a_{33} \cdot la_{21} \cdot z_p + 2 \cdot a_{11} \cdot a_{14} \cdot la_{21} \cdot z_p -$$
$$-2 \cdot a_{11} \cdot a_{14} \cdot a_{31} \cdot z_p + 2 \cdot a \cdot a_{13} \cdot a_{31} - 2 \cdot a \cdot a_{13} \cdot la_{21} - 2 \cdot la_{11}^2 \cdot z_p + 2 \cdot a \cdot a_{33}^2 - 2 \cdot a_{14} \cdot a_{31} \cdot a_{33} \cdot z_p -$$
$$-2 \cdot a_{13} \cdot a_{31} \cdot z_p - 2 \cdot b \cdot a_{13} \cdot a_{33} + 2 \cdot a_{13} \cdot la_{21} \cdot z_p + 2 \cdot b \cdot a_{13} \cdot la_{11} + 4 \cdot a_{11} \cdot la_{11} \cdot z_p + 2 \cdot a_{14} \cdot a_{31} \cdot la_{11} \cdot z_p -$$
$$-2 \cdot a_{14} \cdot la_{11} \cdot la_{21} \cdot z_p - 2 \cdot a_{11}^2 \cdot z_p\Big] \cdot \omega_{e0}\Big\} \cdot \omega_{r0} + la_{11}^2 \cdot a_{33}^2 - 2 \cdot a_{13}^2 \cdot a_{31} \cdot la_{21} + \omega_{e0}^4 +$$
$$+\left(a_{11}^2 - 2 \cdot a_{11} \cdot la_{11} + la_{11}^2 + 2 \cdot a_{13} \cdot a_{31} + a_{33}^2 - 2 \cdot a_{13} \cdot la_{21}\right) \cdot \omega_{e0}^2 + a_{13}^2 \cdot a_{31}^2 + a_{13}^2 \cdot la_{21}^2 + 2 \cdot a_{13} \cdot a_{31} \cdot a_{33} \cdot la_{11} -$$
$$-2 \cdot a_{11} \cdot a_{33}^2 \cdot la_{11} - 2 \cdot a_{13} \cdot a_{33} \cdot la_{11} \cdot la_{21} + a_{11}^2 \cdot a_{33}^2 - 2 \cdot a_{11} \cdot a_{13} \cdot a_{31} \cdot a_{33} + 2 \cdot a_{11} \cdot a_{13} \cdot a_{33} \cdot la_{21}$$

≡ the transfer function afferent to the SOC observer [4]

$$G_2(s) = \frac{\Delta g}{\Delta u} = K_b \cdot \frac{s^3 + \sigma_2 \cdot s^2 + \sigma_1 \cdot s + \sigma_0}{s^4 + \gamma_3 \cdot s^3 + \gamma_2 \cdot s^2 + \gamma_1 \cdot s + \gamma_0} \tag{20}$$

where: $K_b = z_p \cdot a_{14} \cdot k^2 \cdot \underline{\psi}_{r0}^2;\ \underline{\psi}_{r0}^2 = \psi_{dr0}^2 + \psi_{qr0}^2;\ \Delta g = \psi_{qr0} \cdot \Delta e_a - \psi_{dr0} \cdot \Delta e_b;\ \Delta u = \Delta\omega_r - \Delta\hat{\omega}_r;$

$$\omega_{e0} = \omega_0 + \omega_{sl0};\ \sigma_2 = -k \cdot \alpha_2;\ \sigma_1 = \omega_{e0}^2 + k \cdot (k-1) \cdot \omega_0 \cdot \omega_{e0} + k^2 \cdot a_{33} \cdot \alpha_1;\ \sigma_0 = k^2 \cdot \omega_{e0} \cdot \left(\alpha_1 \cdot \omega_0 - \alpha_2 \cdot \omega_{e0}\right)$$

$$\gamma_3 = -2 \cdot k \cdot \alpha_2;\ \gamma_2 = \left(k^4 + 1\right) \cdot \omega_{e0}^2 + k^2 \cdot \omega_0^2 - 2 \cdot k \cdot \left(k^2 - k + 1\right) \cdot \omega_0 \cdot \omega_{e0} + k^2 \cdot \alpha_3;$$

$$\gamma_1 = -2 \cdot k^2 \cdot \Big[\left(k^2 - k + 1\right) \cdot \alpha_2 \cdot \omega_{e0}^2 - \left(k^2 + 1\right) \cdot \alpha_1 \cdot \omega_0 \cdot \omega_{e0}\Big] - 2 \cdot k^3 \cdot \Big[\alpha_1 \cdot \omega_0^2 + a_{33} \cdot \alpha_1 \cdot \alpha_2\Big];$$

$$\gamma_0 = k^4 \cdot \Big[\omega_{e0}^4 - 2 \cdot \omega_0 \cdot \omega_{e0}^3 + \omega_0^2 \cdot \omega_{e0}^2 + \alpha_4 \cdot \omega_{e0}^2 + \alpha_1^2 \cdot \omega_0^2 + a_{33}^2 \cdot \alpha_1^2 - 2 \cdot a_{11} \cdot \alpha_1 \cdot \omega_0 \cdot \omega_{e0}\Big];$$

$$\alpha_1 = a_{11} + a_{14}\cdot a_{31};\ \alpha_2 = a_{11} + a_{33};\ \alpha_3 = \alpha_2^2 + 2\cdot a_{33}\cdot\alpha_1; \alpha_4 = \alpha_2^2 - 2\cdot a_{33}\cdot\alpha_1;\ \omega_0 = z_p\cdot\omega_{r0}.$$

≡ the transfer function afferent to the Gopinath-Peng observer [7]

$$G_3(s) = \frac{\Delta\varepsilon}{\Delta u} = K_c\cdot\alpha_0\cdot\frac{s\cdot(s+\alpha_0)+\omega_{e0}^2}{(s+\alpha_0)^2+\omega_{e0}^2} \tag{21}$$

where: $K_c = \frac{L_m}{L_r}\cdot z_p\cdot\underline{\psi}_{r0}^2;\ \underline{\psi}_{r0}^2 = \psi_{dr0}^2 + \psi_{qr0}^2;\ \Delta u = \Delta\omega_r - \Delta\hat{\omega}_r;\ \Delta\varepsilon = -(a_{33}\cdot\Delta\varepsilon_a + \omega_0\cdot\Delta\varepsilon_b);$

$$\Delta\varepsilon_a = \psi_{dr0}\cdot\Delta e_2 - \psi_{qr0}\cdot\Delta e_1;\ \Delta\varepsilon_b = \psi_{dr0}\cdot\Delta e_1 + \psi_{qr0}\cdot\Delta e_2;\ \alpha_0 = k\cdot\sqrt{a_{33}^2+\omega_0^2}.$$

In order to determine the transfer functions presented above, the following hypotheses were made:

$$\omega_0 = \hat{\omega}_0;\ i_{ds0} = \hat{i}_{ds0}; i_{qs0} = \hat{i}_{qs0};\ \psi_{dr0} = \hat{\psi}_{dr0};\ \psi_{qr0} = \hat{\psi}_{qr0} \tag{22}$$

Taking into account the transfer functions (19), (20) and (21), the simplified block diagrams of the speed observers are shown in Figure 4.

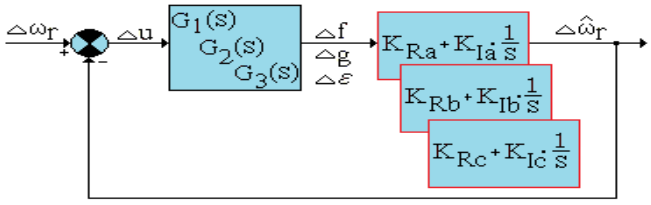

Figure 4. Simplified block diagrams of the speed observers

In order to obtain very good dynamic performances, the adaptation mechanisms from the component of speed observers are defined by the following coefficients:

≡ in the case of the ELO observer [1]

$$K_{Ra} = \frac{1}{K_a\cdot\eta_a};\ K_{Ia} = \frac{K_{Ra}}{\rho_a};\ 0<\rho_a<1;\ 0<\eta_a<1 \tag{23}$$

≡ in the case of the SOC observer [4]

$$K_{Rb} = \frac{1}{K_b\cdot\eta_b};\ K_{Ib} = \frac{K_{Rb}}{\rho_b};\ 0<\rho_b<1;\ 0<\eta_b<1 \tag{24}$$

≡ in the case of the Gopinath-Peng observer [7]

$$K_{Rc} = \frac{1}{K_c};\ K_{Ib} = \frac{K_{Rc}}{\rho_c};\ 0<\rho_c<1 \tag{25}$$

Based on the above, the closed loop transfer functions become:

≡ in the case of the ELO observer

$$G_{01}(s) = \frac{\Delta\hat{\omega}_r}{\Delta\omega_r} = \frac{(\rho_a\cdot s+1)\cdot(\rho_3\cdot s^3+\rho_2\cdot s^2+\rho_1\cdot s+\rho_0)}{\theta_5\cdot s^5+\theta_4\cdot s^4+\theta_3\cdot s^3+\theta_2\cdot s^2+\theta_1\cdot s+\theta_0} \tag{26}$$

where $\theta_5 = \eta_a\cdot\rho_a;\ \theta_4 = \rho_a\cdot(\eta_a\cdot\beta_3+\rho_3);\ \theta_3 = \rho_3+\rho_a\cdot(\eta_a\cdot\beta_2+\rho_2);\ \theta_2 = \rho_2+\rho_a\cdot(\eta_a\cdot\beta_1+\rho_1);$

$$\theta_1 = \rho_1+\rho_a\cdot(\eta_a\cdot\beta_0+\rho_0);\ \theta_0 = \rho_0.$$

≡ in the case of the SOC observer

$$G_{02}(s) = \frac{\Delta\hat{\omega}_r}{\Delta\omega_r} = \frac{(\rho_b\cdot s+1)\cdot(s^3+\sigma_2\cdot s^2+\sigma_1\cdot s+\sigma_0)}{\mu_5\cdot s^5+\mu_4\cdot s^4+\mu_3\cdot s^3+\mu_2\cdot s^2+\mu_1\cdot s+\mu_0} \tag{27}$$

where $\mu_5 = \eta_b\cdot\rho_b;\ \mu_4 = \rho_b\cdot(\eta_b\cdot\gamma_3+1);\ \mu_3 = 1+\rho_b\cdot(\eta_b\cdot\gamma_2+\sigma_2);\ \mu_2 = \sigma_2+\rho_b\cdot(\eta_b\cdot\gamma_1+\sigma_1);$

$$\mu_1 = \sigma_1+\rho_b\cdot(\eta_b\cdot\gamma_0+\sigma_0);\ \mu_0 = \sigma_0.$$

≡ in the case of the Gopinath-Peng observer

$$G_{03}(s) = \frac{\Delta\hat{\omega}_r}{\Delta\omega_r} = \alpha_0\cdot\frac{(\rho_c\cdot s+1)\cdot(s^2+\alpha_0\cdot s+\omega_{e0}^2)}{\xi_3\cdot s^3+\xi_2\cdot s^2+\xi_1\cdot s+\xi_0} \tag{28}$$

where $\xi_3 = \rho_c\cdot(1+\alpha_0);\ \xi_2 = \alpha_0\cdot[1+\rho_c\cdot(2+\alpha_0)];\ \xi_1 = \alpha_0^2\cdot(\rho_c+1)+\rho_c\cdot\omega_{e0}^2\cdot(\alpha_0+1);\ \xi_0 = \alpha_0\cdot\omega_{e0}^2.$

In the following, if we use the stability criterion Routh - Hurwitz, we can make the following statements:

≡ the speed observer (ELO observer) defined by (26), is asymptotically stable if and only if $\rho_0 > 0$. When $\rho_0 < 0$ the speed observer is unstable. From condition $\rho_0 = 0$, we obtain the boundary of the stability domain. The coefficient $\rho_0$ is equal to zero when

$$k=\frac{a_{33}}{a_{11}+a_{33}} \text{ or } k=\frac{R_s\cdot L_r+R_r\cdot L_s}{L_r\cdot R_s}\cdot\left(1+\frac{\omega_{sl0}}{\omega_0}\right) \text{ or } \omega_{e0}=0 \quad (\omega_0=-\omega_{sl0}) \tag{29}$$

≡ the speed observer (SOC observer) defined by (27), is asymptotically stable if and only if $\sigma_0>0$. When the coefficient $\sigma_0$ is strictly negative, the speed observer is unstable. From condition $\sigma_0=0$, we obtain the boundary of the stability domain. The coefficient $\sigma_0$ is equal to zero when

$$\frac{\omega_0}{\omega_{sl0}}=-\frac{R_s\cdot L_r+R_r\cdot L_s}{L_r\cdot R_s} \text{ or } \omega_{e0}=0\,;\,(\omega_0=-\omega_{sl0}) \tag{30}$$

≡ the speed observer (Gopinath-Peng observer) defined by relation (28) is asymptotically stable regardless of the operating mode of the induction machine (regenerating mode or motor mode). This statement is based on the following satisfied properties of the Routh-Hurwitz criterion:

- all coefficients of the polynomial of the poles are positive ($\xi_i>0\,;\,\forall i=0,1,2,3$);
- the next inequality is true

$$H=\xi_2\cdot\xi_1-\xi_3\cdot\xi_0=a_0\cdot\omega_{e0}^2+b_0>0 \tag{31}$$

where $a_0=\alpha_0^3\cdot(\rho_c+1)\cdot\left[\rho_c\cdot(\alpha_0+2)+1\right]>0$; $b_0=\rho_c^2\cdot\alpha_0\cdot(\alpha_0+2)\cdot(\alpha_0+1)>0$.

Figure 5 shows the instability domains of the first 2 speed observers (ELO and SOC). The instability domains are obtained following the graphical representation of the relations $(29)_2$, $(29)_3$ and (30). In this sense, the electrical parameters of a 4 [kW] induction motor are used (see Table 1). The instability domain of the ELO observer was obtained using a proportionality coefficient of $k=1.2$.

From Figure 5, it is observed that the instability domain of the SOC observer (domain represented with yellow) is smaller than the instability domain of the ELO observer (hatched domain). The two domains of instability become equal when:

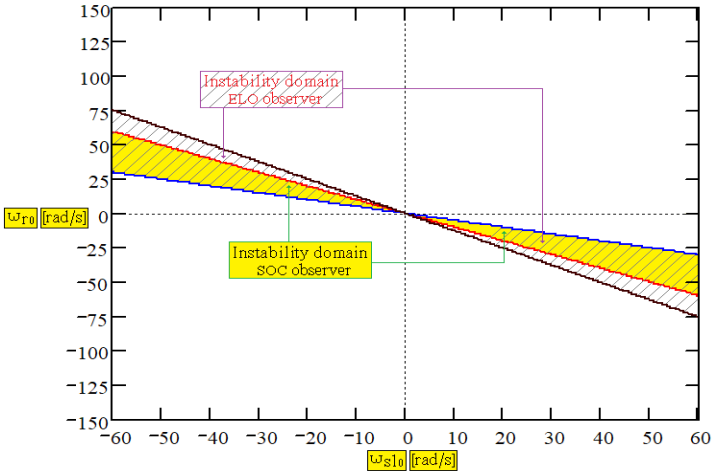


Figure 5. Speed observers instability domains

$$k=-\left(1+\frac{\omega_0}{\omega_{sl0}}\right) \tag{32}$$

To avoid the instability problems of ELO and SOC observers, stabilization algorithms can be used [8], [9]. From the above, it can be seen that the Gopinath-Peng observer does not require a stabilization algorithm.

## 6. SYMULATION RESULTS

The dynamic performances of the three observers previously presented are evaluated by numerical simulation in Matlab - Simulink.

The three observers are tested in sensorless vector control systems. The block diagrams of the sensorless vector control systems is shown in Figure 6.

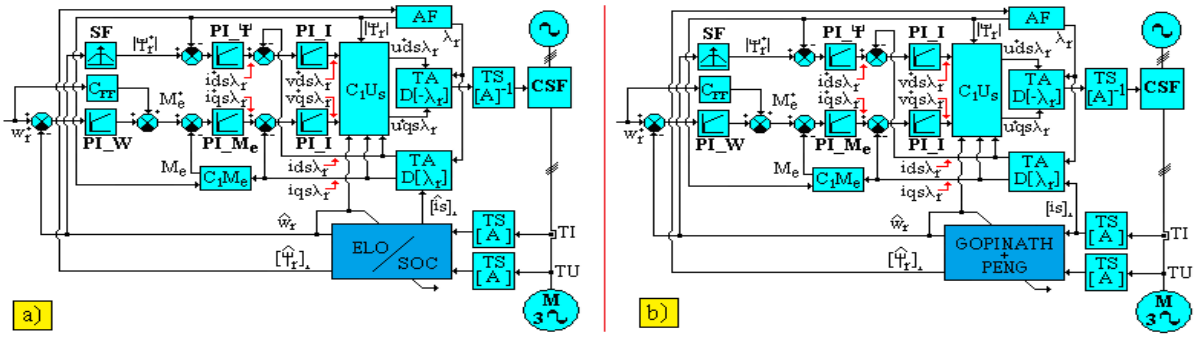


Figure 6. The block diagrams of the sensorless vector control systems
a) the vector control systems used in testing the ELO and SOC observers; b) the vector control systems used in testing the Gopinath-Peng observer.

For the tests by numerical simulation, a 4 [kW] induction motor is used, which has the electrical and mechanical parameters presented in Table 1.

In Figure 6 the following notations were used [1]: TI - are current transducers; TU - are voltage transducers; CSF- is the frequency static converter; AF - is the flux analyzer; $C_1U_s$ - is the stator voltages decoupling block; $C_1M_e$ - is torque calculation block; SF - is the field weakening block; TS - is the direct and inverse Clarke transformation; TA - is the direct and inverse Park transformation, PI - are the five Proportional – Integral type controllers, $C_{FF}$ - is feed forward component of the 2DOF type speed controller. The CSF converter is one with intermediary continuous voltage circuit.

The feed forward component (CFF) of the 2DOF controller is defined so [10], [11]:

$$C_{FF}(s)=\frac{K_0}{s+\omega_0} \tag{33}$$

Table 1. Electrical and mechanical parameters of the induction motor

| Symbol | Name | Value |
|---|---|---|
| $R_s$ | Stator resistance | 1.405 [Ω] |
| $R_r$ | Rotor resistance | 1.395 [Ω] |
| $L_s$ | Stator inductance | 0.178039 [H] |
| $L_r$ | Rotor inductance | 0.178039 [H] |
| $L_m$ | Mutual inductance | 0.1722 [H] |
| J | Motor inertia | 0.0131 [kg·m$^2$] |
| F | Coefficient of friction | 0.002985 [N·m·sec/rad] |
| $n_N$ | Rated speed | 1430 [rpm] |
| $n_e$ | Synchronous speed | 1500 [rpm] |
| $z_p$ | Number of pole pairs | 2 |
| $f_N$ | Rated frequency | 50 [Hz] |
| $U_N$ | Rated voltage | 400 [V] |
| $T_N$ | Rated torque | 26.7 [N·m] |
| $T_F$ | Static friction torque | 3.4 [N·m] |
| $T_{max}/T_N$ | Breakdown torque | 2.3 |

where $K_0=-J\cdot\left(\frac{\omega_0}{2}\right)^2$; $\omega_0=\frac{1}{T}$, $T$ - is the time constant of the vector control system.

The transfer function that defines the five PI-type controllers is

$$G_{PI}(s)=K_{pj}+K_{ij}\cdot\frac{1}{s};\ j=\overline{1,4} \tag{34}$$

Current controllers are defined by the same proportionality and integration constants. In all tests performed by numerical simulation in Matlab-Simulink, the constants that define the controllers in the component of the vector control systems in Figure 6, are the same and are given in Table 2.

Table 2. The parameters of the automatic controllers [12]

| # | Symbol | Name | Value | Obs. |
|---|---|---|---|---|
| 1. | $K_{p1}$ | Constant of proportionality | 370 | The rotor flux controller (PI_Ψ) |
| | $K_{i1}$ | Constant of integration | 2903 | |
| 2. | $K_{p2}$ | Constant of proportionality | 0.1 | The torque controller (PI_$M_e$) |
| | $K_{i2}$ | Constant of integration | 110 | |
| 3. | $K_{p3}$ | Constant of proportionality | 1.3 | The speed controller (PI_W) |
| | $K_{i3}$ | Constant of integration | 33 | |
| 4. | $K_{p4}$ | Constant of proportionality | 11 | The current controllers (PI_I) |
| | $K_{i4}$ | Constant of integration | 2710 | |
| 5. | $\omega_0$ | Natural angular speed | 200 | 2DOF controller |

On the other hand, the proportionality and integration constants that define the adaptation mechanisms of the three observers are given in Table 3.

Table 3. The parameters of the adaptation mechanisms

| Symbol | Name | Value | Obs. |
|---|---|---|---|
| $K_{Ra}$ | Constant of proportionality | 500 | The ELO observer |
| $K_{Ia}$ | Constant of integration | 5000000 | |
| $K_{Rb}$ | Constant of proportionality | 500 | The SOC observer |
| $K_{Ib}$ | Constant of integration | 5000000 | |
| $K_{Rc}$ | Constant of proportionality | 0.4 | The Gopinath-Peng observer |
| $K_{Ic}$ | Constant of integration | 2500 | |

The proportionality constant $k$ has the value 1.2 ($k=1.2$), both in the case of the ELO observer and in the case of the SOC observer. The ELO and SOC observers are simulated without using stabilization algorithms.

In the simulations, the transistors from the CSF component are considered with ideal switching. On the other hand, within the PWM modulator, the carrier is of isosceles triangle type having a frequency of 5 [kHz]. The modulation technique used is the modified subosillation method (over the stators reference voltages is injected the 3rd degree harmonic of the phase voltage, having amplitude of 1/6 of the fundamental reference voltage) [13], [14]. Because the first frequency which appears in the stator voltages spectrum is the triangular waveform

frequency, both the currents and the stator voltages will be filtered with two pole Butterworth filters, which have de cutoff frequency set 500 [Hz].

The tests for determining the dynamic performances of the mentioned observers, are performed in the area of low speeds (±60 rpm) when the induction motor has zero load torque ($T_L = 0[N \cdot m]$).

All simulations are done in Matlab-Simulink, using the Dormand – Prince integration method (ode45), which has a relative and absolute error of: $err = 10^{-6}$.

The results of the simulations are presented in the following figures.

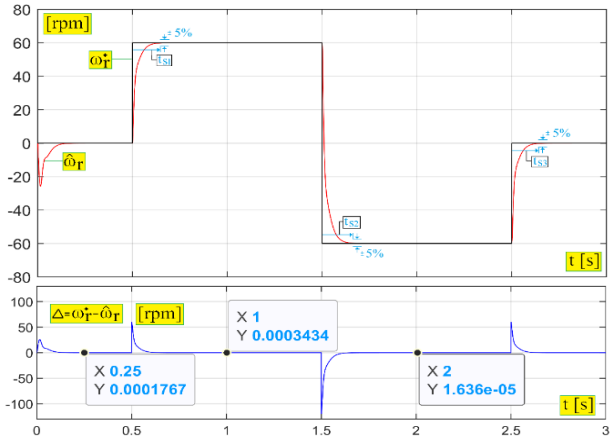


Figure 7. The speed response – ELO observer

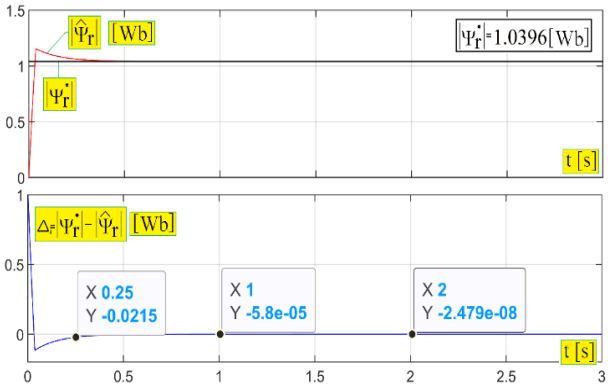


Figure 8. The rotor flux space vector response – ELO observer

Following the tests by numerical simulation, as well as figures 7 and 8, we can say the following conclusions:

- the settling times of the speed response of ELO observer, are: ts1≈0.07 [s]; ts2≈0.09 [s]; ts3≈0.1[s];
- the peak value of the estimate rotor flux space vector is 1.1573 [Wb] (thus, the maximum overshoot is: $\sigma_{ELO} \approx 11.32[\%]$);
- the steady-state errors in the case of the speed response of ELO observer are $\varepsilon_{st}(t_1) \approx 1.7 \cdot 10^{-4}\,[rpm]$; $\varepsilon_{st}(t_2) \approx 3.4 \cdot 10^{-4}\,[rpm]$; $\varepsilon_{st}(t_3) \approx 1.6 \cdot 10^{-5}\,[rpm]$; where $t_1 \approx 0.25[s]$; $t_2 \approx 1[s]$; $t_3 \approx 2[s]$;
- the steady-state errors in the case of the rotor flux space vector response of ELO observer are: $e_{st}(t_1) \approx -2.1 \cdot 10^{-2}\,[Wb]$; $e_{st}(t_2) \approx -5.8 \cdot 10^{-5}\,[Wb]$; $e_{st}(t_3) \approx 2.4 \cdot 10^{-8}\,[Wb]$.

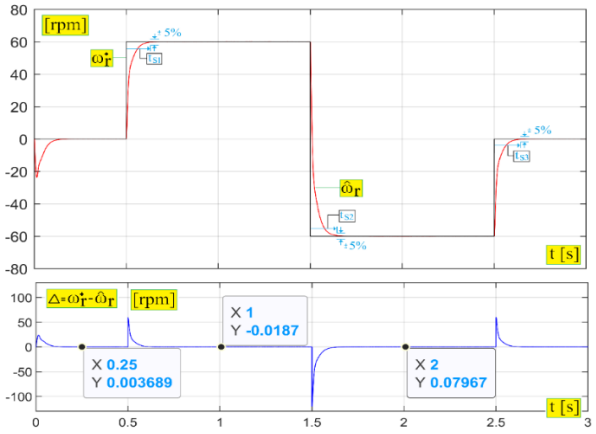


Figure 9. The speed response – SOC observer

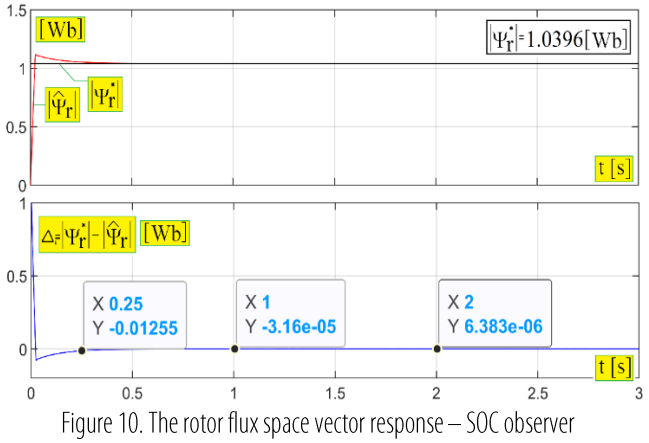


Figure 10. The rotor flux space vector response – SOC observer

The main conclusions obtained from the numerical simulation test of the SOC observer are:

- the settling times of the speed response of SOC observer are the same as in the case of the ELO observer;
- the peak value of the estimate rotor flux space vector is 1.1204 [Wb] (thus, the maximum overshoot is: $\sigma_{SOC} \approx 7.7[\%]$);
- the steady-state errors in the case of the speed response of SOC observer are $\varepsilon_{st}(t_1) \approx 3.6 \cdot 10^{-3}\,[rpm]$; $\varepsilon_{st}(t_2) \approx -1.8 \cdot 10^{-2}\,[rpm]$; $\varepsilon_{st}(t_3) \approx 7.9 \cdot 10^{-2}\,[rpm]$;
- the steady-state errors in the case of the rotor flux space vector response of SOC observer are: $e_{st}(t_1) \approx -1.255 \cdot 10^{-2}\,[Wb]$; $e_{st}(t_2) \approx -3.1 \cdot 10^{-5}\,[Wb]$; $e_{st}(t_3) \approx 6.3 \cdot 10^{-6}\,[Wb]$.

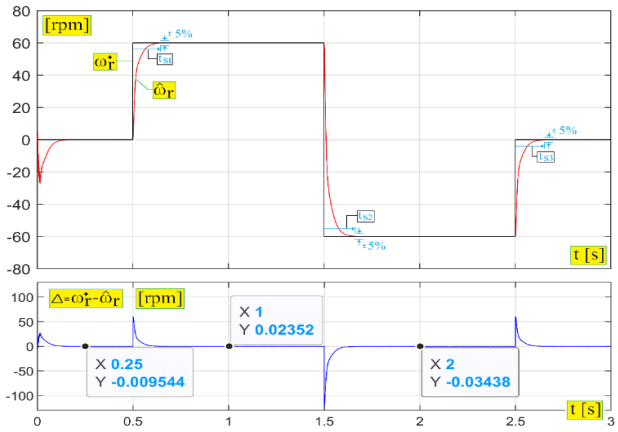

Figure 11. The speed response – Gopinath – Peng observer

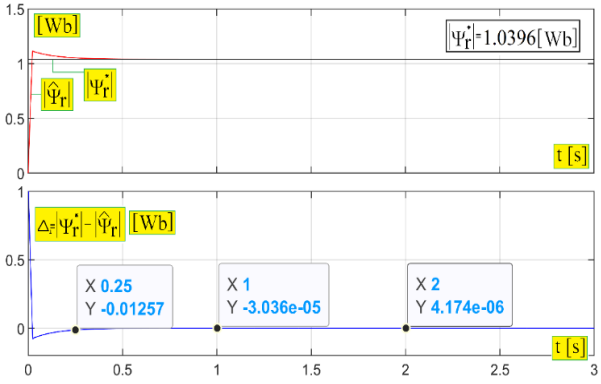

Figure 12. The rotor flux space vector response – Gopinath – Peng observer

Similarly, following the simulation of the Gopinath-Peng observer, the following conclusions were obtained:

- the settling times of the speed response of Gopinath -Peng observer are the same as in the case of the ELO and SOC observers;
- the peak value of the estimate rotor flux space vector is 1.1186 [Wb] (thus, the maximum overshoot is: $\sigma_{GP} \approx 7.5[\%]$);
- the steady-state errors in the case of the speed response of Gopinath-Peng observer are $\varepsilon_{st}(t_1) \approx -9.5 \cdot 10^{-3}\,[rpm]$; $\varepsilon_{st}(t_2) \approx 2.3 \cdot 10^{-2}\,[rpm]$; $\varepsilon_{st}(t_3) \approx -3.4 \cdot 10^{-2}\,[rpm]$;
- the steady-state errors in the case of the rotor flux space vector response of Gopinath-Peng observer are: $e_{st}(t_1) \approx -1.257 \cdot 10^{-2}\,[Wb]$; $e_{st}(t_2) \approx -3 \cdot 10^{-5}\,[Wb]$; $e_{st}(t_3) \approx 4.1 \cdot 10^{-6}\,[Wb]$.

On the other hand, from the tests performed it was observed that when the imposed speed is maintained at zero for more than 8 seconds, both the ELO observer and the SOC observer become unstable, so that the orientation after the rotor flux space vector is lost.

In the following, we will make a classification of the observers presented, according to the steady-state errors. In this sense, we will introduce a set of notes, between 1 and 3 (the note 1 is for the best performance, and note 3 is for the weakest performance).

Thus, the classification of the observers presented according to the steady-state errors of the speed response, are in Table 4.

Table 4. Classification of observers according to steady-state errors - $\varepsilon_{st}$

| Observers | $\lvert\varepsilon_{st}(t_1)\rvert$ | $\lvert\varepsilon_{st}(t_2)\rvert$ | $\lvert\varepsilon_{st}(t_3)\rvert$ | Final classification ($FC_1$) |
|---|---|---|---|---|
| ELO | 1 | 1 | 1 | 1 |
| SOC | 2 | 2 | 3 | 2 |
| Gopinath-Peng | 3 | 3 | 2 | 3 |

On the other hand, in Table 5 is presented the classification of the presented observers, according to the steady-state errors of the response of rotor flux space vector.

Table 5. Classification of observers according to steady-state errors - $e_{st}$

| Observers | $\lvert e_{st}(t_1)\rvert$ | $\lvert e_{st}(t_2)\rvert$ | $\lvert e_{st}(t_3)\rvert$ | Final classification ($FC_2$) |
|---|---|---|---|---|
| ELO | 3 | 3 | 1 | 3 |
| SOC | 1 | 2 | 3 | 2 |
| Gopinath-Peng | 2 | 1 | 2 | 1 |

In order to achieve an even more concise classification, in addition to the previous criteria, we will introduce two more:

- the stability of the observer (SO);
- maximum overshoot of the estimate rotor flux space vector (σ).

Thus, in Table 6 is presented a final classification of the observers presented, according to all the previously mentioned criteria.

Table 6. Final classification of observers - ELO; SOC and Gopinath-Peng

| Observers | $FC_1$ | $FC_2$ | SO | σ | Final classification (FC) |
|---|---|---|---|---|---|
| ELO | 1 | 3 | 3 | 3 | 3 |
| SOC | 2 | 2 | 2 | 2 | 2 |
| Gopinath-Peng | 3 | 1 | 1 | 1 | 1 |

The previously presented research can be extended in the future, taking into account other criteria such as:

- the parametric sensitivity of the observers (SP). In this sense, the sensitivity of the observers to the variations of the rotor resistance and the stator resistance of the induction motor can be tested.
- sensitivity of observers to measurement noises (SN);
- the criteria presented in the article, when the induction motor is operated in load etc.

Based on the criteria taken into account (see Table 6), we can say that the Gopinath-Peng observer has the best dynamic performance, followed by the SOC observer and the ELO observer.

## 7. CONCLUSIONS

The article presents a comparative analysis of three adaptive observers that can be used in sensorless vector control systems. The comparative analysis was performed by numerical simulation in Matlab-Simulink. The observers analyzed are: ELO, SOC and Gopinath-Peng. These observers are able to simultaneously estimate the speed as well as the d-q components of the rotor flux space vector of an induction motor. Following the comparative analysis, the general conclusion is that the Gopinath-Peng observer has better dynamic performances than the SOC and ELO observers.

The results obtained in this article can be a basis in choosing the most convenient type of observer that can be used in a sensorless vector control system. In addition, the article also presents some future research directions for a more accurate classification of the three observers.

**Note**: This paper was presented at CNAE 2022 – XX$^{th}$ National Conference of Electric Drives, organized by University POLITEHNICA Timisoara, Faculty of Faculty of Electrotechnics and Electroenergetics (ROMANIA), in Timisoara, ROMANIA, in 12-13 May, 2022

## References

[1] T. Pana, O. Stoicuta, "The stability of vectororial control systems with induction motors", Mediamira Publishing House, Cluj-Napoca, 2016.
[2] H. Kubota, K. Matsuse, T. Nakano, "DSP-based speed adaptive flux observer of induction motor", in IEEE Transactions on Industry Applications, vol. 29, no. 2, pp. 344-348, March-April 1993.
[3] O. Stoicuta, T. Pana, "New adaptive observer for sensorless induction motor drives", Annals of the Univ. Eftimie Murgu of Resita, no.2, pp.175-186, 2014.
[4] O. Stoicuta, "Design and Analysis a Speed and Rotor Flux Observer for Sensorless Vector Control Systems of Induction Motors", 2021 9th International Conference on Modern Power Systems (MPS), 2021, pp. 1-10.
[5] H. Tajima, Y. Hori, "Speed Sensorless Field Orientation Control of the Induction Machine", IEEE Trans. Ind. Application, vol.29, no.1, pp.175-180,1993.
[6] F.Z.Peng, T.Fukao, "Robust speed identification for speed-sensorless vector control of induction motors", in IEEE Transactions on Industry Applications, vol. 30, no. 5, pp. 1234-1240, Sept.-Oct. 1994.
[7] O. Stoicuta, "Speed and Rotor Flux Estimation using Back-EMF MRAS and Gopinath Observers for Sensorless Vector Control Systems of Induction Motors", 2021 9th International Conference on Modern Power Systems (MPS), 2021, pp. 1-8.
[8] H. Kubota, I. Sato, Y. Tamura, K. Matsuse, H. Ohta and Y. Hori, "Regenerating-mode low-speed operation of sensorless induction motor drive with adaptive observer", in IEEE Transactions on Industry Applications, vol. 38, no. 4, pp. 1081-1086, July-Aug. 2002.
[9] T. Pana and O. Stoicuta, "Design of an extended Luenberger observer for sensorless vector control of induction machines under regenerating mode", 2010 12th International Conference on Optimization of Electrical and Electronic Equipment, 2010, pp. 469-478.
[10] L. Harnefors, S. E. Saarakkala and M. Hinkkanen, "Speed Control of Electrical Drives Using Classical Control Methods", in IEEE Transactions on Industry Applications, vol. 49, no. 2, pp. 889-898, March-April 2013.
[11] A. Gogea, O. Stoicuta and T. Pana, "Comparative Analysis Between the PI Speed Controller and Two-Degrees-of-Freedom Speed Controller for Induction Motor Drive", 2019 8th International Conference on Modern Power Systems (MPS), 2019, pp. 1-6.
[12] T. Pana and O. Stoicuta, "Controllers tuning for the speed vector control of induction motor drive systems", 2010 IEEE International Conference on Automation, Quality and Testing, Robotics (AQTR), 2010, pp. 1-6.
[13] J. Holtz, "Pulsewidth modulation for electronic power conversion", in Proceedings of the IEEE, vol. 82, no. 8, pp. 1194-1214, Aug. 1994.
[14] O. Stoicuta, "The Utilization of the S-Function Block in Simulation of the Luenberger Rotor Flux Observer for Induction Motors", Annals of the University of Petrosani Electrical Engineering, vol. 18, pp. 31-46, 2016.



ISSN 1584 – 2665 (printed version); ISSN 2601 – 2332 (online); ISSN-L 1584 – 2665